Photodetachment of Deprotonated R-Mandelic Acid: The Role of Proton Delocalization on the Radical Stability

Franco Molina, Rafael Jara-Toro, Jennifer Noble, Claude Dedonder-Lardeux, Christophe Jouvet, Gustavo Ariel Pino

Photodetachment of Deprotonated *R*-Mandelic Acid: The Role of Proton Delocalization on the Radical Stability

Mr. Franco L. Molina,[a,b,c] Dr. Rafael A. Jara-Toro,[a,b,c] Dr. Jennifer A. Noble,[d] Dr. Claude Dedonder-Lardeux[d] and Dr. Christophe Jouvet[d] and Prof. Gustavo A. Pino,[a,b,c,*]

a- INFIQC : Instituto de Investigaciones en Fisicoquímica de Córdoba (CONICET – UNC) - Haya de la Torre s/n, Ciudad Universitaria, X5000HUA Córdoba, Argentina.

b- Departamento de Fisicoquímica, Facultad de Ciencias Químicas – Universidad Nacional de Córdoba – Haya de la Torre y Medina Allende, Ciudad Universitaria, X5000HUA Córdoba, Argentina.

c- Centro Láser de Ciencias Moleculares - Universidad Nacional de Córdoba - Haya de la Torre s/n, Pabellón Argentina, Ciudad Universitaria, X5000HUA Córdoba, Argentina.

d- Physique des Interactions Ioniques et Moléculaires (PIIM): CNRS, Aix-Marseille Université, Marseille, France.

* Corresponding author: gpino@unc.edu.ar

https://infiqc-fcq.psi.unc.edu.ar/personal/pino-gustavo-ariel/

Abstract

The photodetachment and stability of R-Mandelate, the deprotonated form of the R-Mandelic acid, was investigated by observing the neutral species issued from either simple photodetachment or dissociative photodetachment in a cold anions set-up. R-Mandalate has the possibility to form an intramolecular ionic hydrogen-bond between adjacent hydroxyl and carboxylate groups. The potential energy surface along the proton transfer (PT) coordinate between both groups (O^-…H^+…$^-$OCO) features a single local minima, with the proton localized on the O^- group (OH…$^-$OCO). However, the structure with the proton localized on the $^-$OCO group (O^-…HOCO) is also observed because it falls within the extremity of the vibrational wavefunction of the OH…$^-$OCO isomer along the PT coordinate. The stability of the corresponding radicals, produced upon photodetachment, is strongly dependent on the position of the proton in the anion: the radicals produced from the OH…$^-$OCO isomer decarboxylate without barrier, while the radicals produced from the O^-…HOCO isomer are stable.

Introduction

Carboxylic acids (RCOOH) and their corresponding deprotonated carboxylates ($RCOO^-$) are extensively used as substrates in biological and chemical syntheses. Particularly, the radical decarboxylative functionalization is of high interest as a synthetic method.[1-3]

Many strategies have been employed to induce the decarboxylation and, since 2008, visible-light-induced photoredox catalysis has emerged as a powerful method for initiating radical reactions under very mild reaction conditions and low-energy irradiation.[3-6] This strategy has resulted in a significant advancement in the field of synthetic organic chemistry.

The process starts with the absorption of a photon by the carboxylate anion ($RCOO^-$), leading to electron detachment (ED) and the formation of the intact carboxylic radical ($RCOO^\bullet$) (reaction R.1). The carboxylic radical can be stable or spontaneously decarboxylate to produce the corresponding aryl or alkyl radical ($R^\bullet$) and CO_2 (reaction R.2).

$$RCOO^- + h\nu \rightarrow RCOO^\bullet + e^- \qquad (R.1)$$

$$RCOO^\bullet \rightarrow R^\bullet + CO_2 \qquad (R.2)$$

The combination of R.1 and R.2 is called dissociative photoelectron detachment (DPD).

In addition, if the first excited states of $RCOO^-$ lie below the ED threshold, photon absorption can promote the electron to an electronically excited state of the anion followed by internal conversion to the ground electronic state that finally leads to ionic fragmentation (reaction R.3).

$$RCOO^- + h\nu \rightarrow R^- + CO_2 \qquad (R.3)$$

Given the richness of the photoproducts that can be observed ($RCOO^\bullet$, $R^\bullet$ and R^-) and the fact that they will lead to different synthetic products, it is important to understand the underlying mechanism controlling the yields of reactions R.1, R.2 and R.3, at the molecular level.

These processes and the competition between them can be investigated at the molecular level using laser spectroscopy of isolated, gas phase molecular ions in a mass-spectrometer experimental set-up. When possible, the anions can also be cooled

down to achieve higher spectroscopic resolution and a better control of the internal energy.

In this regard, DPD has been observed as the main process upon UV excitation of many small anions and recent progress on this topic can be found in a review by Continetti et al.[7] The DPD of the acetyl carboxylate anion ($CH_3CO_2^-$) has been studied by coincidence experiments and both the intact acetyloxy radical (R.1) as well as its fragments have been observed, and a barrier of 0.2 eV in the exit channel for the dissociation into $CO_2 + CH_3^\bullet$ was estimated.[8]

As mentioned above, R.3 has been observed in the case of aryl carboxylate anions with optically active excited states that lie lower in energy than the Adiabatic Detachment Energy (ADE), as observed for the green fluorescent protein chromophore (p-hydroxybenzylidene-2,3-dimethylimidazolone),[9-11] the naphtoate anion,[12] the phthalate anion[13] and some aromatic sulfonate and phosphate anions.[14]

Others carboxylate anions have also been studied by IR and UV spectroscopies, for example benzoate ($C_6H_5COO^-$), whose photoexcitation leads to decarboxylation either in the ground state of the anion or in the radical.[12,15] Remarkably, when a second carboxylic group is present in the anion, as in the case of phthalate anion, bi-decarboxylation was observed, leading to $C_6H_5^- + 2\ CO_2$.[13]

The aromatic amino acids tyrosine and tryptophan can be considered as aromatic alcohols, phenol or indole (RXH, with X = O or N, respectively) with a carboxylic acid group. These compounds can be deprotonated either on the carboxylic acid group ($(XH)RCOO^-$) or on the alcoholic XH group ($(^-X)RCOOH$).[16]

The excitation of the most stable isomer $(XH)RCOO^-$ above the ADE leads to formation of the $(XH)RCOO^\bullet$ radical which is unstable and decomposes via decarboxylation into $(XH)R^\bullet + CO_2$. On the contrary, the excitation of the higher energy $(^-X)RCOOH$ isomer above the ADE produces a stable $(^\bullet X)RCOOH$ radical that does not dissociate on the experimental timescale.[16]

These findings indicate that further work is still needed to establish how the presence of additional functional groups on the aryl-carboxylate anions will affect the competition between R.1, R.2 and R.3.

A question arising from previous results on tyrosine and tryptophan anions is how an intramolecular hydrogen bond (HB) between the –XH or $-X^-$ and the –COOH or $–COO^-$ groups can affect the stability/decarboxylation of the resulting radical.

HBs are ubiquitous throughout nature. Particularly interesting is the ionic HB that is characterized by a strong interaction energy and is responsible for many structural motifs found in several chemical and biological systems.[17]

Intramolecular (neutral or ionic) HBs are involved in hydrogen or proton transfer (HT/PT) reactions which are ubiquitous in chemistry and biochemistry. It has been stablished that the stronger the HB, the lower the barrier for the HT/PT.[18]

The ionic HB has been extensively investigated at the molecular level in cold ions using different chemical systems. Of special interest is the proton shared by two neutral molecules ($A\ldots H^+\ldots B$)[19 - 26] as well as that shared by two anionic moieties ($A^-\ldots H^+\ldots B^-$). [19,27 - 30] In these cases, much effort has been made to determine the H^+ position and, especially, whether the proton is shared between A and B (A^- and B^-) or localized on a single moiety, being A and B different or the same molecule.[13,19 - 33]

Due to the low mass of H/H^+ and the usually low energetic barriers associated with HT/PT, nuclear quantum effects (NQEs) must be considered in order to achieve a more precise description of the structure and dynamics of the system, as observed in many examples reported in bibliography.[13,21-27,27,31-33]

R-Mandelic acid ($C_8H_8O_3$) is a chiral aromatic alpha hydroxy acid soluble in water and polar organic solvents that was first obtained from extracts of bitter almonds and serves as a substrate for the synthesis of various compounds in the pharmaceutical and dermatological industries.[34]

R-Mandelate ($C_8H_7O_3^-$) (Scheme 1), the deprotonated form of this acid, has the possibility to form an intramolecular ionic HB between the hydroxyl group and the carboxylate group (O-H…$^-$OCO), giving access to an experimental system that allows us to answer the question posed above.

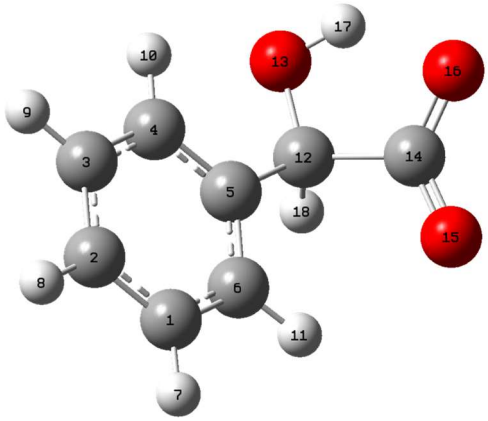

Scheme 1: *Molecular structure and atomic number labels of R-Mandelate ($C_8H_7O_3^-$).*

In this work, we present a study of the UV photoexcitation of cold R-Mandelate, and the energy dependence of the yields of R.1, R.2 and R.3, by collecting the yield of the neutral and ionic fragments as well as the intact precursor radical as a function of the excitation energy. The experiments are interpreted with the aid of quantum calculations.

Methodology

Experimental

R-Mandelate anions ($C_8H_7O_3^-$) were produced in an electrospray source (ESI) source by injecting a solution of R-Mandelic acid at $2x10^{-4}$ M in a 1:1 mixture of methanol:water.

The experimental setup for cold ion photofragmentation spectroscopy[21,35,36] has been modified to detect neutral particles and negative ions as was already described in previous publications.[12-14,16]

Briefly, the ions produced in the ESI source are injected into the quadrupole-ion-trap (QIT) just after a helium pulse has been introduced. The ions are stored in the cold QIT for a few tens of ms, the time necessary for cooling to c.a. 30 K and decreasing the pressure in the trap. The ions are then extracted and accelerated at 2.6 kV; the voltage of the extracting electrode of the trap and the accelerating grid are adjusted to fulfill the Wiley McLaren focusing conditions.[37] After the accelerating grid, the ions enter the Gauss tube set at the accelerating grid potential and, once they are inside, the tube is switched to ground. The ions then travel in the field-free region of the time of flight (TOF) mass spectrometer with a kinetic energy due to the accelerating voltage and they are referenced to the ground potential.

In most of the experiments, the laser interacted with the parent anions in the Gauss tube. Since the parent anions ($RCOO^-$) have already been accelerated, the neutral parent radicals produced after photodetachment ($RCOO^\bullet$) and/or the neutral daughter fragments ($R^\bullet$, CO_2, etc.) can be detected by the MCP (multichannel plate). The intact parent radical will arrive at the same time as the parent anion and the signal will be as narrow as the anion signal. In contrast, the neutral fragments will travel with the kinetic energy of the parent anion plus the kinetic energy (positive or negative) released in the dissociative process, so that they will be observed at the same TOF as the parent but with a peak broadening due to kinetic energy release.

As shown in previous publications, the TOF profile of neutral particles is composed of a central narrow peak corresponding to the unfragmented radical and broad wings on both sides of the central peak due to neutral products of dissociation processes.[12-14,16]

To discriminate between the parent anion and the parent neutral photodetached radical the voltage on the Gauss tube was kept on in order to decelerate the anions at the output of the tube and prevent them from reaching the detector without perturbing the neutrals. This method minimizes the time and the distance travelled by the parent

ions and thus reduces the background signal from neutral fragments produced by collisions of the parent ion with the residual gas.

Some experiments were also performed allowing the laser to interact with the anions in the QIT, which allows monitoring of the photodissociation process, leading to a daughter ion and one or more neutral fragments, by extracting the ions after the laser shot.

To record the spectra, the excitation laser (a tunable OPO laser from EKSPLA, 10 Hz repetition rate, 10 ns pulse width and a spectral resolution of ~ 10 cm^{-1}) was scanned in the 410 – 225 nm spectral range with 0.5 nm steps. For each point, prior to stepping the wavelength the signal is averaged over 8 laser shots.

The TOF distributions that characterize the signal of neutral particles were symmetrized following the procedure described in recent publications.[16]

Calculations

The structure and stability of different isomers of the $C_8H_7O_3^-$ anion were calculated using density functional theory (DFT) with the CAM-B3LYP functional and the aug-cc-pVDZ basis set[38] using the Gaussian 16 suite of programs.[39] The Adiabatic (ADE) and Vertical (VDE) Detachment Energies were also calculated at the same level of theory. Vertical transition energies to electronically excited states of the anion and the corresponding oscillator strengths (OS) were calculated using the time-dependent DFT formalism (TD-DFT) with the same functional and basis set as used for the ground state calculations.

Results and Discussion

Experimental

The symmetrized TOF profiles of the neutrals obtained by the interaction of the laser with $C_8H_7O_3^-$ in the Gauss tube at different photon energies are shown in Figure 1. The TOF profiles of the neutral species are composed of two kinds of peaks: a narrow one, which has the width of the parent signal (i.e. 20 ns) and corresponds to the intact neutral ($C_8H_7O_3^{\bullet}$) radical produced by photodetachment (R.1) and two broad peaks with a width of a few hundreds of nanoseconds that correspond to neutral fragments (R.2).

The symmetrized TOF were fitted using the same procedure described in previous works.[12,16] The fitting was achieved with a combination of one Gaussian function whose width is the same as the width of the parent anion peak, i.e. 20 ns and accounts for the narrow peak, and two step-functions accounting for the two neutral

fragments (broad peaks). In Figure 1 it can be observed that the yield of the fragmentation channel increases as the excitation energy increases.

From the fit of the experimental data, we extract the mean widths of the two broad peaks (322 ± 40 ns and 900 ± 50 ns), which remain unchanged as a function of the excitation energy. If we assume that the dissociation channel corresponds to CO_2 loss, as in the case of other aromatic acid anions,[12,13,16] the ratio of the widths of the two broad peaks, 0.36 ± 0.07, reflects the mass ratio of the two neutral fragments $m_{CO_2}:m_{C_7H_7O^{\bullet}}$ = 0.41. Considering the widths of the peaks and the geometry of the TOF mass spectrometer and following the procedure described in previous publications,[12-14,16] the kinetic energy released in the dissociation process is estimated as (0.30 ± 0.04) eV.

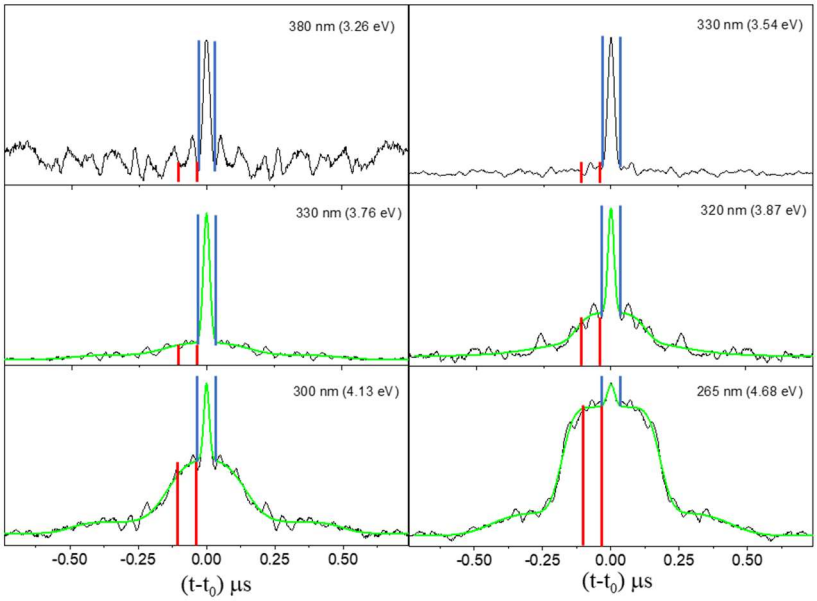

Figure 1: *Typical TOF profiles, normalized to the maximum signal at (t-t_0) = 0 μs, of the neutrals generated from the interaction of the laser with cold $C_8H_7O_3^-$ anions (40K) in the Gauss tube at the various photon energies given in the panel labels. (dots,* **o***) Experimental data points, (line, ——) fit to a Gaussian function corresponding to intact $C_8H_7O_3^{\bullet}$ radicals and two step-functions corresponding to $C_7H_7O^{\bullet}$ and CO_2 fragments. For excitation spectra (Figure 2), the laser energy is scanned while the detection is set to different arrival time intervals to monitor the intact radical (narrow peak between blue bars corrected by subtracting the component due to the broad peak lying underneath) or the fragments (broad peak detected between the red bars).*

The excitation spectra shown in Figure 2 were obtained by scanning the photon energy in the 3.0 – 5.4 eV spectral range while recording the area under different arrival time intervals of the TOF profiles. The arrival time interval for the fragments was set between the vertical red bars in the broad peak (Figure 1) leading to the excitation spectrum in red (Figure 2) and the arrival time interval for the intact parent radical was set between the vertical blue bars (Figure 1) leading to the excitation spectrum in blue (Figure 2). In the case of the intact parent radical, the signal between the blue bars was

corrected by subtracting the component due to the broad peak lying underneath (red bars).

The spectrum recorded on the signal corresponding to the intact $C_8H_7O_3^{\bullet}$ radical shows the photodetachment threshold at (3.17 ± 0.02) eV (391 ± 2 nm) followed by an unstructured band with a maximum at 3.5 eV (354 nm) and whose intensity becomes negligible at 4.3 eV (288 nm) with an apparent second threshold above this energy.

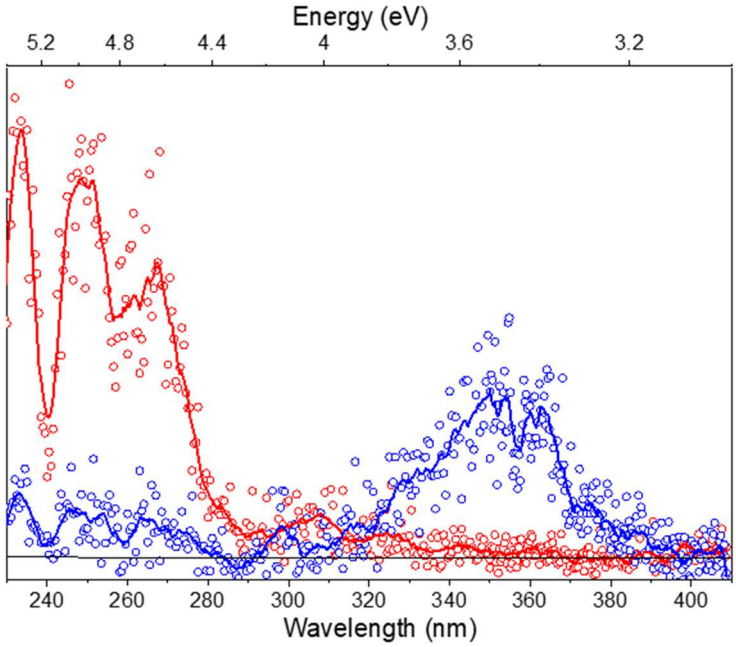

Figure 2: *Excitation spectra recorded while scanning the laser with the detection set either on the stable unfragmented radical ($C_8H_7O_3^{\bullet}$, blue) or on the neutral fragment ($C_7H_7O^{\bullet}$, red). The stable radical is detected at times between the blue bars of the TOF peak depicted in Figure 1, while the fragment is detected on the broad part of the TOF peak i.e. at times between the red bars in the same Figure. The signal for the stable radical (blue trace) has been corrected by subtracting the contribution of the broad peaks lying underneath the narrow peak.*

In the case of the spectrum recorded on the signal of the neutral fragments (red), it shows the onset at (3.55 ± 0.05) eV (349 ± 5 nm) that monotonically increases up to 4.3 eV (288 nm), where it presents a sudden enhancement of the fragments signal as the excitation energy increases, probably due to a second threshold.

With the aim of studying the direct photofragmentation from the electronically excited anions leading to anionic fragments, experiments were also performed allowing the laser to interact with the anions in the QIT as in previous works.[12-14] With this experimental set-up we were unable to observe any anionic fragments, suggesting that the direct ionic fragmentation channel is closed or negligible in the spectral region explored.

Theoretical

The $C_8H_7O_3^-$ anion exists in several isomeric forms including two deprotonation sites as in the case of the aromatic amino acids tyrosine and tryptophan:[16] the deprotonation of the carboxylic group (–COOH), that will be called ManCOO$^-$, and the deprotonation of the –OH group localized on the side chain, that will be called ManO$^-$. In turn, both isomers show two rotamers, one of them has an intramolecular H-bond (OH…COO$^-$ or O$^-$…COOH) which is not allowed for the other rotamer. They will be distinguished by the notation "1" for the H-bonded and "2" for the non-H-bonded.

Table 1 shows the structure of the four isomers with the calculated relative energies including zero point energy correction (EE+ΔZPE) and the corresponding VDE and ADE.

Table 1: *Structures and relative electronic energy (EE) of the four isomers of the $C_8H_7O_3^-$ anion without and with zero point energy correction (ZPE). Vertical and adiabatic electron detachment energies (ADEs and VDEs). All energy values are given in eV.*

Label	Structure	EE [eV]	VDE [eV]	ADE [eV]
Man1COO$^-$	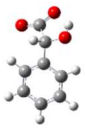	0	4.36	4.15
Man2COO$^-$	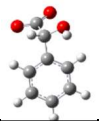	0.65	3.91	3.62
Man1O$^-$	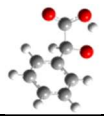	0.63[a]		3.43
Man2O$^-$		1.44	2.84	2.61

[a] The reported EE for Man1O$^-$ is the lowest EE obtained for this isomer, obtained when starting the optimization from the vertical structure of the optimized Man1O$^•$ and keeping the O16-H17 bond distance fixed to 0.975 Å, as shown in Table SI2.

The global minimum corresponds to the Man1COO$^-$ isomer. However, this isomer does not seem to correspond to the experimentally observed species because the calculated ADE = 4.15 eV is 0.98 eV higher than the lowest experimental threshold (3.17 eV) observed on the signal of the intact $C_8H_7O_3^•$ radical.

In the case of the Man1COO$^{\bullet}$ radical isomer, the determination of the ADE was not direct as the optimization of a stable radical structure required a stepwise approach. The optimization of Man1COO$^{\bullet}$, starting from the structure of optimized Man1COO^{-} leads to the elimination of CO_2 as a consequence of the C12-C14 bond breaking in the first optimization step, even when setting the size for the optimization step to the smallest possible (0.01 Bohr or radians). In order to get an optimized structure of the radical, two strategies were used: 1) the C12-C14 bond length was fixed to 1.571 Å as in the optimized structure of the anion and 2) the optimization was started from a structure slightly distorted as compared to the vertical structure. In both cases, the optimization was achieved in two optimization steps, reaching the same optimized geometry. The most relevant geometrical parameters are reported in Table SI1 (Supplementary Material).

The Man2COO^{-} isomer is located at 0.65 eV from the global minimum with a calculated ADE = 3.62 eV, which is in close agreement with the first experimental threshold. However, Man2COO$^{\bullet}$ is also unstable and spontaneously eliminates CO_2, as in the case of Man1COO$^{\bullet}$. Therefore, neither Man1COO$^{\bullet}$ nor Man2COO$^{\bullet}$ is the stable radical experimentally observed in the energy range 3.17 – 4.30 eV.

The instability of this type of radical against decarboxylation has been previously reported for other aromatic carboxylic acids.[12,13] Similar behavior was reported for the case of the deprotonated amino acids tyrosine and tryptophan.[16] In those anions, it was determined that the deprotonation of the carboxylic group leads to anions whose corresponding radicals are unstable and decarboxylate without any energy barrier. However, the deprotonation of the OH groups in the indole or phenol side-chain led to anions that form stable radicals upon electron detachment.

Based on this insight, the hypothesis that the excitation of Man1O^{-} and/or Man2O^{-} isomers could be responsible for the observation of the intact $C_8H_7O_3^{\bullet}$ radical was considered. However, the optimization of the Man1O^{-} isomer was found to be unfeasible because it led to the most stable Man1COO^{-} isomer within the first optimization steps, suggesting that there is no barrier to intramolecular proton transfer (PT) from the -CO_2H group to the -O^{-} group. In fact, it was not possible to find any transition state (TS) for the PT in the anion potential energy surface.

The Man2O^{-} anion could be optimized, because the proton on the -CO_2H group points away from the -O^{-} group, but this structure lies very high in energy (1.44 eV) compared to the other isomers; thus, it is not expected to be populated at the temperature of the experiment. In addition, the calculated ADE = 2.61 eV and VDE = 2.84 eV lie significantly below the first experimental threshold (3.17 ± 0.02 eV).

Therefore, considering the fact that in Man1O$^-$ the proton could be delocalized between the -COO$^-$ and the -O$^-$ groups, a relaxed scan of the O16-H17 bond distance in the anion was performed and the vertical energies for the corresponding radicals at each O16-H17 bond distance were also calculated. The schematic potential energy curves for the anion and radical are shown in Figure 3 in filled black squares and filled green circles, respectively.

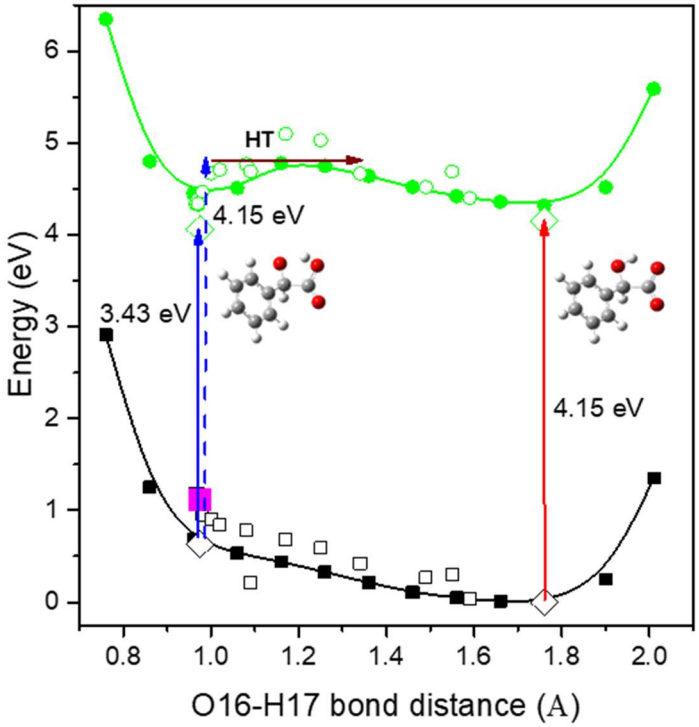

Figure 3: *Potential energy curve for the anion (black) and the radical (green) along the O16-H17 bond distance. The relaxed scan was performed in the anion with the initial O13-C12-C14-O16 dihedral angle set at 0° (filled square) and at 60 ° (open square). The energy curve in the radical was built on the vertical energies from the anions. The calculated ADE (reported in Table 1) are shown as open diamonds and are indicated by the vertical arrows for Man1O$^-$ (blue) and Man1COO$^-$ (red). The vertical dashed blue arrow indicates the excitation energy at which the HT barrier is overcome in the radical. The pink square corresponds to the vertical energy of the Man1O$^-$ anion calculated from the optimized structure of the Man1O$^\bullet$ radical.*

In the anion, one imaginary frequency corresponding to the O16-H17 stretching mode was observed throughout the scan, with all other calculated frequencies being positive. The exceptions to this was the point at O16-H17 = 1.76 Å (O13-H17 = 0.99 Å) corresponding to the structure of the global minimum for which all frequencies were positive. The O13-C12-C14-O16 dihedral angle remained close to 0° upon optimization along the O16-H17 scan.

In addition to the imaginary frequency associated with the O16-H17 stretch, in the point-by-point vertical energy calculation in the radical a second imaginary frequency was observed in all the structures, associated with the distortion of the O13-C12-C14-O16 dihedral angle. Therefore, a second relaxed scan of the O16-H17 bond distance

was performed, but starting with the O13-C12-C14-O16 dihedral angle set to 60°. The result of this scan is also shown in Figure 3 in open black squares and open green circles for the anion and radical, respectively.

Although qualitatively, the results of both scans are the same, the minor differences suggest that the proton delocalization and radical decarboxylation reactions involve multiple coordinates and they deserve further theoretical approaches at higher levels of theory.

From the moderate theory level used in this work, it is observed that in the anion the proton (H17) delocalizes between O13 and O16 without encountering any energy barrier. However, in the radical the barrier for the intramolecular hydrogen transfer (HT) between O13 and O16 is 0.7 eV, as estimated from these scans.

Calculations aimed to search for the TS for the HT in the radical were also performed. The energy barrier is found at 0.12 eV above the most stable Man1O$^{\bullet}$ radical. However, as shown in Table SI3, this TS corresponds to the coupled HT and C12-C14 bond scission and does not represents the actual HT coordinate.

It is known that the PT/HT barrier, characteristic of a weak HB between neutrals - such as in the case of the radical - becomes either absent or very low in strong ionic HBs, as in the case of the anion.[18,19]

The presence of the barrier to HT in the radical allowed the optimization of Man1O$^{\bullet}$ with an EE = 4.06 eV (Table SI2). Therefore, the EE of Man1O^{-} was derived using two approaches: as the vertical energy from the optimized Man1O$^{\bullet}$ as well as by optimization of Man1O^{-} keeping the O16-H17 bond distance fixed to 0.975 Å. The results are shown in Table SI2. The latter method renders the lowest energy for the Man1O^{-} (0.63 eV) and this value was used to calculate the ADE of Man1O^{-} as (3.43 eV) (Table 1) which is in close agreement with the first experimental threshold (3.17 ± 0.02) eV observed on the signal of the intact $C_8H_7O_3^{\bullet}$ radical.

On the contrary, in the anion the absence of any barrier to the PT between Man1O^{-} and Man1COO^{-} allows proton delocalization across both moieties.

The phenomenon of proton delocalization as a consequence of a shallow potential energy surface allowing proton translocation has been reported in several anionic systems containing ionic HBs (e.g. the proton-bound dimer of hydrogen sulfate and formate $[HSO_4^{-}\ldots H^{+}\ldots CHOO^{-}]^{-}$,[27] deprotonated phthalic acid $[C_6H_4(CO_2^{-})_2H^{+}]^{-}$,[13] deprotonated dicarboxylic acids $[(CH_2)_n(CO_2^{-})_2H^{+}]^{-}$ (n= 2-4),[40] etc.). In those systems, nuclear quantum effects need to be considered in order to explain the observed spectroscopy. In this sense, classical molecular dynamics simulations using the many-body polarizable AMOEBA force field in combination with a two-state empirical valence-

bond (EVB) to allow for proton transfer, has satisfactorily reproduced the experimental IR spectra of dicarboxylic acids $[(CH_2)_n(CO_2^-)_2H^+]^-$ (n= 2-4) at different temperatures.[40]

To evaluate the stability of Man1COO$^\bullet$ and ManO$^\bullet$ toward decarboxylation, a relaxed scan along the C12-C13 bond distance was performed for both radicals and the results are shown in Figure 4. In the case of Man1COO$^\bullet$ the dissociation of the C12-C13 bond leading to CO_2 elimination proceeds without an energy barrier, confirming that this isomer cannot be responsible for the observation of the stable $C_8H_7O_3^\bullet$ radical. However, as shown in Figure 4.b, Man1O$^\bullet$ exhibits an energy barrier of 0.2 eV along the C12-C13 bond distance coordinate; as such, it is stable in close proximity to the ADE geometry and could thus, be responsible for the observation of the intact radical.

Given these results, the experimental data can be interpreted by considering that the first threshold (3.17 ± 0.02) eV observed in the signal of the intact radical corresponds to the ADE of Man1O$^-$ calculated at 3.43 eV, which produces the Man1O$^\bullet$ radical. According to the calculations, Man1O$^\bullet$ is stable toward decarboxylation with a barrier of 0.2 eV for the C12-C14 dissociation and shows a barrier of 0.7 eV for the intramolecular HT leading to the unstable Man1COO$^\bullet$ isomer. The Man1O$^-$ anion is unstable along the O16-O17 PT coordinate and that geometry will return to the geometry of Man1COO$^-$. Man1O$^-$ can only be observed if we consider that it falls within the extremity of the vibrational wavefunction of Man1COO$^-$ along the PT coordinate.

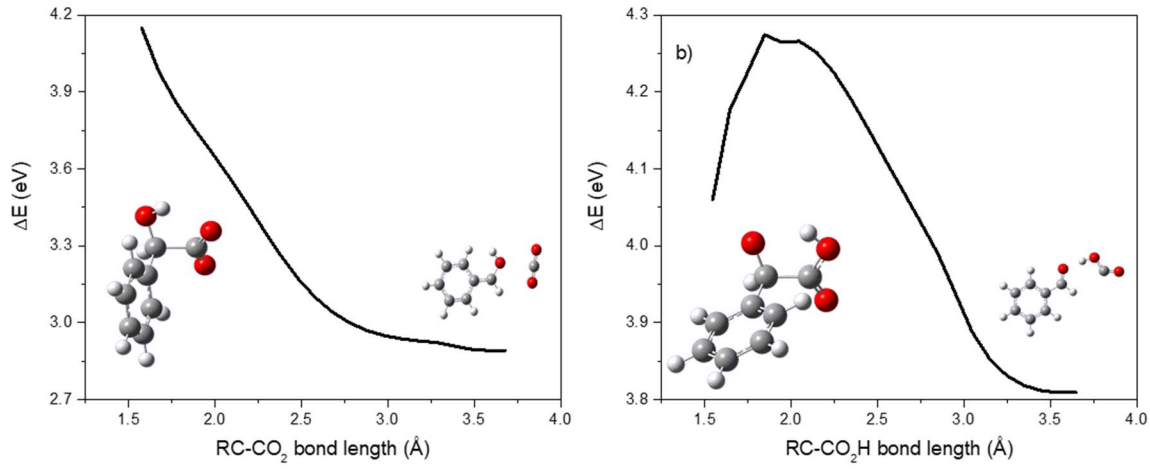

Figure 4: *Potential energy curve for Man1COO$^\bullet$ (a) and Man1O$^\bullet$ (b) radicals along the C12-C14 reaction coordinate, leading to CO_2 or HOCO elimination, respectively. The barrier for Man1O$^\bullet$ decomposition in b) is 0.2 eV.*

The fact that the experimental spectrum recorded on the intact radical signal shows a threshold at (3.17 ± 0.02) eV and reaches a maximum at (3.55 ± 0.05) eV

suggests a barrier for the radical decomposition of around 0.38 eV, in agreement with the calculated barrier (0.2 eV).

The experimental fragmentation threshold at (3.55 ± 0.05) eV could be also overlapped with the direct excitation of the Man2COO$^-$ isomer near its ADE = 3.62 eV and both processes are observed in the same energy range.

Finally, the sudden enhancement of the signal recorded on the neutral fragments above 4.3 eV (red trace in Figure 2) is associated with the direct excitation of the most stable and populated Man1COO$^-$ isomer near its ADE (calculated at 4.15 eV) and considering that the Man1COO$^\bullet$ radical is unstable toward decarboxylation.

As shown in Table 2, the vertical transition energies to electronically excited states of the three anions are found to lie in the 4.2 - 5.2 eV energy region and thus these transitions could also contribute to the experimental band observed at 4.3 eV.

Excitation to electronically excited states of the anions would be expected to lead to anionic fragments.[12-14] As mentioned in the experimental results section, we were unable to observe any anionic fragments when the experiment was performed in the QIT. Therefore, excitation to electronically excited states of the anions can be dismissed as being responsible for this experimental band (3.55 eV). This is also in line with previous studies in which it was observed that anionic fragments produced following excitation to electronically excited states of the anion are only observed when the states lie at energies below the ADE,[12-14] which is not the case in this system.

Table 2: *Vertical electronic transition energies for the first four singlet excited states of the three anions and the corresponding oscillator strengths (OS). The calculations were performed at the TD-DFT level using the CAM-B3LYP functional with the aug-cc-pVDZ basis set.*

Isomer	Vertical Electronic Transition Energies and Oscillator Strengths			
	S_1	**S_2**	**S_3**	**S_4**
Man1COO$^-$	4.74 eV OS: 3x10^{-3}	4.91 eV OS: 1x10^{-2}	5.09 eV OS: 1x10^{-2}	5.17 eV OS: 7x10^{-3}
Man2COO$^-$	4.26 eV OS: 1x10^{-3}	4.26 eV OS: 1x10^{-3}	4.49 eV OS: 3x10^{-3}	4.62 eV OS: 4x10^{-2}
Man1O$^-$	4.20 eV OS: 2x10^{-3}	4.35 eV OS: 6x10^{-3}	4.39 eV OS: 7x10^{-3}	4.51 eV OS: 2x10^{-3}

Conclusions

The electron photodetachment and radical fragmentation of the cold R-Mandelate anion was studied experimentally by detecting the neutral particles (intact radical or neutral fragments) produced because of the interaction of the cold anion with the laser radiation. These data were compared to quantum chemical calculations describing the various isomeric forms of the anion and radical.

The experimental results are rationalized by considering that the most stable isomer Man1COO$^-$ (deprotonated on the carbonyl group) absorbs photons above 4 eV and is unstable upon electron detachment, leading to two neutral fragments CO_2 and $C_7H_7O^\bullet$.

The signal of the intact radical observed at low excitation energy does not correspond to Man1COO$^-$ but to Man1O$^-$, the isomer deprotonated on the OH group of the side-chain. The corresponding Man1O$^\bullet$ radical is stable toward decarboxylation and isomerization to the unstable Man1COO$^\bullet$ radical at excitation energies close to the ADE because of the presence of energy barriers for these processes.

The Man1O$^-$ isomer is unstable along the intramolecular PT coordinate because of the absence of any barrier to this process. Thus, it can only be observed if we consider that it falls within the extremity of the vibrational wavefunction of Man1COO$^-$ along the PT coordinate.

Therefore, it is worth noting that, in this type of experiment, the experimental results cannot always be explained by considering only stable structures, and that quantum effects must also be considered. Molecular dynamics simulations allowing for PT, such as EVB-AMOEBA model,[40] would be of great interest in order to fully understand the present system.

Although the theoretical calculations presented in this work allow for a rationalization of the experimental results, ideally, higher levels of theory would be desired in order to obtain a better quantitative comparison. Such an approach would also provide a good opportunity to test the validity of high level theoretical methods for this type of molecular system, but is outside the scope of the current study.

Acknowledgments

This work was conducted within the International Associated Laboratory LEMIR (CNRS/CONICET) and was supported by CONICET, FONCyT, SeCyT-UNC, MinCyt-Córdoba and the ANR Research Grant (ANR2010BLANC040501-ESPEM).

Keywords: Cold anions spectroscopy - Density functional calculations - Laser spectroscopy - Mass spectrometry - Nuclear quantum effects.

Conflict of Interest:

There are no conflicts to declare.

Twitter: @infiqcenred

Reference

[1] A. J. J. Straathof, *Chem. Rev.* **2014**, *114*, 1871.

[2] L. J. Gooßen, N. Rodríguez, K. Gooßen, *Angew. Chem., Int. Ed.* **2008**, *47*, 3100.

[3] J. Xuan, Z-G. Zhang, W-J. Xiao, *Angew. Chem. Int. Ed.* **2015**, *54*, 15632.

[4] J. M. R. Narayanam, C. R. J. Stephenson, *Chem. Soc. Rev.* **2011**, *40*, 102.

[5] C. K. Prier, D. A. Rankic, D. W. C. MacMillan, *Chem. Rev.* **2013**, *113*, 5322.

[6] M. Peña-López, A. Rosas-Hernández, M. Beller, *Angew. Chem. Int. Ed.* **2015**, *54*, 5006.

[7] R. E. Continetti, H. Guo, *Chem. Soc. Rev.*, **2017**, *46*, 7650.

[8] Z. Lu, R. E. Continetti, *J. Phys. Chem. A*, **2004**, *108*, 9962.

[9] M. W. Forbes, R. A. Jockusch, *J. Am. Chem. Soc.*, **2009**, *131*, 17038.

[10] M. W. Forbes, A. M. Nagy, R. A. Jockusch, *Int. J. Mass. Spectrom.*, **2011**, *308*, 155.

[11] S. B. Nielsen, A. Lapierre, J. U. Andersen, U. V. Pedersen, S. Tomita, L. H. Andersen, *Phys. Rev. Lett.*, **2001**, *87*, 228102.

[12] G. A. Pino, R. A. Jara-Toro, J. P. Aranguren-Abrate, C. Dedonder-Lardeux, C. Jouvet, *Phys. Chem. Chem. Phys.* **2019**, *21*, 1797.

[13] E. Marceca, J. A. Noble, C. Dedonder-Lardeux, C. Jouvet, *J. Phys. Chem. A*, **2021**, *125*, 7406.

[14] J. A. Noble, E. Marceca, C. Dedonder-Lardeux, I. Carvin, E. Gloaguen, C. Jouvet, *Eur. Phys. J. D* **2021**, *75*, 95.

[15] J. D. Steill, J. Oomens, *J. Phys. Chem. A* **2009**, *113*, 4941.

[16] J. A. Noble, J. P. Aranguren-Abate, C. Dedonder-Lardeux, C. Jouvet, G. A. Pino, *Phys. Chem. Chem. Phys*. **2019**, *21*, 23346.

[17] M. Meot-Ner, *Chem. Rev.* **2005**, *105*, 213.

[18] M V Basilevsky, M V Vener, *Russ. Chem. Rev.* **2003**, *72*, 1.

[19] N. Heine, K. R. Asmis, *Int. Rev. Phys. Chem.* **2015**, *34*, 1.

[20] J. R. Roscioli, L. R. McCunn, M. A. Johnson, *Science* **2007**, *316*, 249.

[21] G. Féraud, M. Berdakin, C. Dedonder, C. Jouvet, G. A. Pino, *J. Phys. Chem. B* **2015**, *119*, 2219.

[22] A. F. Cruz-Ortiz, M. Rossa, F. Berthias, M. Berdakin, P. Maitre, G. A. Pino, *J. Phys. Chem. Lett.* **2017**, *8*, 5501.

[23] R. Cheng, T. D. Fridgen, E. Loire, J. Martens, *Phys. Chem. Chem. Phys.* **2020**, *22*, 2999.
[24] M. B. Burt, T. D. Fridgen, *J. Phys. Chem. A* **2007**, *111*, 10738.
[25] W. Fu, J. Xiong, M. J. Lecours, P. J. J. Carr, R. A. Marta, E. Fillion, T. McMahon, V. Steinmetz, W. S. Hopkins, *J. Molec. Spectrosc.*, **2016**, *330*, 194.
[26] M. Demireva, J. Oomens, G. Berden, E. R. Williams, *ChemPlusChem,* **2013**, *78*, 995.
[27] D. A. Thomas, M. Taccone, K. Ober, E. Mucha, G. Meijer, G. von Helden, *J. Phys. Chem. A* **2021**, *125*, 9279.
[28] J. J. Kreinbihl, N. C. Frederiks, S. E. Waller, Y. Yang, C. J. Johnson, *J. Chem. Phys.* **2020**, *153*, 034307.
[29] G. –L. Hou, X. -B. Wang, *Acc. Chem. Res.* **2020**, *53*, 2816.
[30] N. Heine, T. I. Yacovitch, F. Schubert, C. Brieger, D. M. Neumark, K. R. Asmis, *J. Phys. Chem. A* **2014**, *118*, 7613.
[31] J. Lin, E. Pozharski, M. A. Wilson, *Biochemistry* **2017**, *56*, 391.
[32] E. G. Diken, J. M. Headrick, J. R. Roscioli, J. C. Bopp, M. A. Johnson, A. B. McCoy, *J. Phys. Chem. A* **2005**, *109*, 1487.
[33] O. Gorlova, J. W. DePalma, C. T. Wolke, A. Brathwaite, T. T. Odbadrakh, K. D. Jordan, A. B. McCoy, M. A. Johnson, *J. Chem. Phys.* **2016**, *145*, 134304.
[34] R. Sarkar, S. Ghunawat, V. K. Garg. *J. Cutan. Aesthet. Surg.* **2019**, *12*, 158.
[35] I. Alata, J. Bert, M. Broquier, C. Dedonder, G. Feraud, G. Grégoire, S. Soorkia, E. Marceca, C. Jouvet, E. Marceca and C. Jouvet, *J. Phys. Chem. A* **2013**, *117*, 4420.
[36] G. Féraud, C. Dedonder, C. Jouvet, Y. Inokuchi, T. Haino, R. Sekiya, T. Ebata, *J. Phys. Chem. Lett.* **2014**, *5*, 1236.
[37] W. C. Wiley, I. . McLaren, *Rev. Sci. Instrum.* 1955, **26**, 1150.
[38] D. E. . Woon, T. H. Dunning Jr., *J. Chem. Phys.* **1993**, *98*, 1358.
[39] Gaussian 16, Revision C.01, M. J. Frisch, G. W. Trucks, H. B. Schlegel, G. E. Scuseria, M. A. Robb, J. R. Cheeseman, G. Scalmani, V. Barone, G. A. Petersson, H. Nakatsuji, X. Li, M. Caricato, A. V. Marenich, J. Bloino, B. G. Janesko, R. Gomperts, B. Mennucci, H. P. Hratchian, J. V. Ortiz, A. F. Izmaylov, J. L. Sonnenberg, D. Williams-Young, F. Ding, F. Lipparini, F. Egidi, J. Goings, B. Peng, A. Petrone, T. Henderson, D. Ranasinghe, V. G. Zakrzewski, J. Gao, N. Rega, G. Zheng, W. Liang, M. Hada, M. Ehara, K. Toyota, R. Fukuda, J. Hasegawa, M. Ishida, T. Nakajima, Y. Honda, O. Kitao, H. Nakai, T. Vreven, K. Throssell, J. A. Montgomery, Jr., J. E. Peralta, F. Ogliaro, M. J. Bearpark, J. J. Heyd, E. N. Brothers, K. N. Kudin, V. N. Staroverov, T. A. Keith, R. Kobayashi, J. Normand, K. Raghavachari, A. P. Rendell, J. C. Burant, S. S. Iyengar, J. Tomasi, M. Cossi, J. M. Millam, M. Klene, C. Adamo, R. Cammi, J. W. Ochterski, R. L. Martin, K. Morokuma, O. Farkas, J. B. Foresman, and D. J. Fox, Gaussian, Inc., Wallingford CT, 2016.
[40] F. Thaunay, F. Calvo, E. Nicol, G. Ohanessian, C. Clavaguéra, *ChemPhysChem* **2019**, *20*, 803.

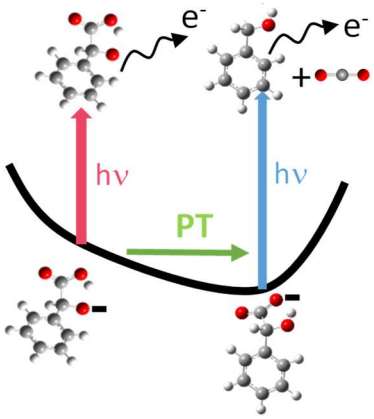

The stability of the radical produced by photodetachment, toward decarboxylation, depends on the deprotonation site of the precursor anion. The anion leading to the stable radical is observed because it falls within the extremity of the vibrational wavefunction, of the most stable anionic structure, along the PT coordinate.